Technoscience Journal for Community Development in Africa 5:1 (2026) 33–48
ISSN 2659-0573

Research Article

Corrosion performance evaluation of Bi-layered Zn/Zn-ZnO-$CaCO_3$ composite coatings on mild steel under marine conditions

Ruth Nkiruka Nnaji[1], Muideen Adebayo Bodude[1], David Ehigie Esezobor[1], Jeleel Adekunle Adebisi[2]

[1]Department of Metallurgical & Materials Engineering, University of Lagos, Lagos, Nigeria
[2]Department of Materials & Metallurgical Engineering, University of Ilorin, Ilorin, Nigeria

Abstract: Research interest has grown in the use of waste-derived calcium carbonate ($CaCO_3$) as eco-friendly additives to zinc (Zn) composite coatings for corrosion protection. The corrosion of bi-layered Zn/Zn-ZnO-$CaCO_3$ composite coatings electrolytically co-deposited on mild steel using biogenic periwinkle shell (PS) and eggshell (ES) wastes was investigated in this study. Using a design of experiments (DoE) framework, the electrodeposition process was optimized focusing on nano-$CaCO_3$ incorporation and uniform coating thickness. Electrochemical frequency modulation (EFM) was used to validate marine corrosion performance of bi-layered Zn/Zn-ZnO-$CaCO_3$ composite coatings, and weight loss was used to assess microbiologically influenced corrosion (MIC) susceptibility in the presence of *Proteus mirabilis*. However, corrosion of single-layer Zn coatings was assessed using potentiodynamic polarisation. Lowest corrosion rate (*CR*) of 0.007 mm/year, coating efficiency (E_{EFM}) of 93.15%, and polarisation resistance (*Rp*) of 59,260.17 Ω.cm^2 was observed at 4.56 g ES nano-$CaCO_3$ addition. Scanning electron microscopy (SEM) showed dense and compact morphology; energy dispersive x-ray spectroscopy (EDS) revealed the presence of oxygen (O), calcium (Ca) and Zn. Results obtained reveal a synergy between Zn, ZnO, and nano-$CaCO_3$ leading to enhanced marine corrosion protection. The developed Zn/Zn-ZnO-$CaCO_3$ composite coating exhibits a strong potential for green, sustainable solutions in corrosion and surface engineering applications.

Keywords: Bi-layered Zn/Zn-ZnO-$CaCO_3$, composite coatings, corrosion, marine, mild steel.

1. Introduction

Mild steel, a metallic alloy of primarily iron (Fe) and carbon (C), is extensively used in shipbuilding and marine engineering applications for ship hull fabrication and offshore structural constructions owing to its desirable mechanical strength and excellent weldability. However, vulnerability of mild steel to accelerated corrosion in marine environments limits the reliability of structural steel assets (Melchers, 2005; Popoola et al., 2016). Additionally, a basic electrochemical corrosion mechanism—a galvanic cell formation on the metal's surface where oxidation and reduction (redox) reactions occur simultaneously—controls surface corrosion of mild steel structures exposed to seawater immersion, such as underwater ship hull plates (Melchers, 2007; Liao et al., 2012). High conductivity (salinity) and dissolved oxygen are the main triggers of marine corrosion mechanism of mild steel in subsurface (near-surface) seawater (de La Fuente et al., 2015; Refait et al., 2018).

Moreover, acidic metabolites produced beneath microbial biofilms and the deposits of microorganisms, such as sulphate-reducing bacteria (SRB), create oxygen differential cells on the metal surface (Chohan et al., 2024; Liu et al., 2024). These cells facilitate the anodic dissolution of iron (Fe) in uncoated (unprotected) mild steel (Xu et al., 2013; Jia et al., 2017). Furthermore, bio-fouling and increased surface roughness occur due to the attachment of macroorganisms, such as barnacles, to submerged mild steel surfaces in near-surface seawater. This results in general (uniform) corrosion with related

* Corresponding author:
Email: ruthnkirukannaji@gmail.com

KWASU PRESS AND PUBLISHING

microbiologically influenced corrosion (MIC), a marine corrosion sub-mechanism of mild steel (Wu et al., 2016; Margapuram et al., 2024).

Traditionally, sacrificial zinc (Zn) or polymeric (epoxy) barrier coatings are applied to mild steel surfaces to prevent marine corrosion. While conventional zinc coatings provide sufficient sacrificial protection in atmospheric conditions, they corrode more quickly in marine seawater (Schmidt et al., 2006; Liu et al., 2017). Notably, the thickness of the zinc-based coating greatly influences mild steel's long-term corrosion resistance in marine environments (Idora et al., 2014). Conventional marine coatings, such as polymeric or epoxy paints, offer moisture barrier protection but do not offer sacrificial protection from electrochemical corrosion mechanism or stop bioaccumulation on steel surfaces in underwater marine environments (Benea et al., 2018). Furthermore, existing marine antifouling coatings contain toxic corrosion inhibiting compounds such as zinc phosphate ($Zn_3(PO_4)_2$), copper (Cu^{2+}), arsenic (As) and other biocides, which leach into seawater, disrupt marine ecosystems and pose risks to aquatic life (Lamprakou et al., 2023; Liu et al., 2022). Thus, it is vital to develop biocompatible, multifunctional composite coatings that provide environmentally safe and sustainable engineering solutions for marine corrosion protection of mild steel.

Calcium carbonate ($CaCO_3$), a fundamental component of corals and shells, exists in three major mineral forms of aragonite, calcite and vaterite. Periwinkle shell and eggshell are rich sources of aragonite and calcite. Calcium carbonate, is an eco-friendly material with the potential to improve the corrosion resistance of Zn composite coated mild steel in marine environment (Nnaji et al., 2023). This study focuses on the marine corrosion susceptibility of bi-layered Zn/Zn-ZnO-$CaCO_3$ ternary composite coatings electrolytically co-deposited on mild steel. The research quantified the performance impact of utilising marine-based local biowaste of periwinkle shell and biogenic eggshell waste as a unit and blend mix of nano-$CaCO_3$ particles to modify a-Zn-ZnO matrix bi-layer on a single-layer zinc first coat on structural mild steel for improved marine corrosion protection of mild steel. A design of experiments (DoE) approach was employed to optimise the electrolytic co-deposition procedure in order to achieve uniform coating thickness and nano-$CaCO_3$ inclusion.

Electrochemical performance of electrodeposited Zn-eggshell (calcined) particles composite coatings on mild steel has been studied in simulated subsea water using linear polarisation resistance (LPR) technique (Aigbodion & Akinlabi, 2019). Anti-corrosion properties of Zn eggshell particle starch-modified composite coatings on mild steel in seawater-simulated solution has been investigated using linear polarisation resistance (Aigbodion & Onuoha, 2024). Corrosion resistance of precipitated $CaCO_3$ (PCC) recovered from asphalt-solid wastes (ashbuton) used as reinforcement in Zn coatings electrodeposition on mild steel has been evaluated in simulated biodiesel environment using electrochemical impedance spectroscopy technique (Fardilah et al., 2025). Corrosion protection of mild steel using polymer-modified ZnO nanoparticles with inhibitor in composite coatings have been reported (Kamburova et al., 2021).

While eggshell and $CaCO_3$ particles have been previously studied in Zn composite coatings, most reported Zn-eggshell electrodeposited coatings were single-layered and used calcined eggshell particles in micro meter sizes. Very limited research had explored bi-layered architectures or the use of nano-$CaCO_3$ particles derived from both periwinkle shell and eggshell biogenic wastes. Valorising periwinkle shell and eggshell biowastes into materials for composite coating fabrication promotes green surface engineering solutions in materials science and corrosion engineering by bridging the gap between waste management and materials sustainability. Through the creation of innovative materials for society's benefits, this study promotes wealth generation from waste and waste burden reduction from environments to create smart cities free from pollution.

2. Materials and methods

2.1. $CaCO_3$ Nanoparticles synthesis and production

Periwinkle shell and eggshell wastes were obtained from local and domestic sources. Periwinkle shells were roughly crushed, washed using clean tap water, and subsequently soaked in 50:50 hydrogen peroxide (3 %) to water solution for about 45 minutes to remove odour and organic matter remains; followed by several washing using hot water, cold water rinsing; and finally, sun-drying. ES processing followed repeated washing using hot and warm water; and then sun-drying. Roughly crushed PS was further ground using a local industrial pulveriser, but ES was initially ground using a domestic blender mill. Partially ground particles of the shells were further milled into fine powders (one at a time) using a planetary ball mill (Model: JC-QM-2; Factory number: JC2021-072367; Manufacturer: Qingdao

Juchuang Environmental Protection Group Co., Ltd., China). The PS and ES powders were separately sieved using ≤150 nm sieve to obtain nano $CaCO_3$ particles. X-ray Diffractometry (XRD) was carried out during pilot investigations to determine the $CaCO_3$ phases in the PS and ES powders.

2.1.1. Substrate preparation

Mild steel plate and zinc anode utilised in the present study were both received from Naval Dockyard Limited (NDL– a Marine Engineering and Shipbuilding Company in Victoria Island, Lagos, Nigeria). Preliminary investigations of microstructure and elemental composition of the as-received steel plate were carried out using optical microscopy and electron spectrometry respectively; the purity of the zinc anode block (99.57 % pure zinc) was determined using Olympus Delta Professional Handheld XRF metal analyzer (Model/Series: DPO-2000; Serial number: 540723; Manufactured in 2014 by Olympus Scientific Solutions Americas Corp.). The as-received mild steel pieces were dimensioned to 50 × 20 × 2 mm rectangular specimens and prepared in triplicates for the electrodeposition processes. Specimens' surfaces were ground using silicon carbide paper (60 to 600 grit sizes), and polished using 0.3 µm and 0.05 µm alumina polishing powders on polishing cloths in succession.

2.1.2. Seawater physicochemical analysis

Physicochemical properties of the electrolyte solutions (surface and subsurface seawater) as well as the nutrient broth used in the study were measured using Horiba U-5000G (HGS No. NFR2LC6V, Power LR14 1.5 V ×4) made in Japan water quality monitor.

2.2 Bath formulation for Zn and Zn-ZnO-$CaCO_3$ electrodeposition on mild steel

The basic bath composition for the Zn and Zn-ZnO-$CaCO_3$ composite coatings electrodeposition on mild steel comprised $ZnSO_4{\cdot}7H_2O$ + $NaSO_4$ + H_3BO_3. The Zn sulphate bath formulation from optimized DoE is summarized in Table 1. $ZnSO_4{\cdot}7H_2O$ was the primary electrolyte salt, $NaSO_4$ was a supporting salt, H_3BO_3 was buffer; $SC(NH_2)_2$ and $C_6H_{12}O_6$ served as brighteners in the coating bath.

Zn coating electrodeposition on mild steel was performed at optimized conditions of temperature (45 °C), voltage (1.4 V), time (60 mins), and no stirring on all mild steel specimen sets; and $CaCO_3$ incorporation into Zn-ZnO matrix for the bi-layered coatings development on Zn-coated mild steel was carried out at the optimized conditions of current density, $CaCO_3$ mass concentration, and time established using a central composite design (CCD) of experiment of Stat-Ease DesignExpert® Version 12.0. Optimal mass concentration of mass of 4.56 g $CaCO_3$/0.35 L was established from CCD randomized electrolytic co-deposition study. 4.56 g of PS and ES nano-$CaCO_3$ as unit particles as well as blend mix particles were incorporated into the composite coating bath one at a time.

Table 1: Bath formulation for Zn and Zn-ZnO-$CaCO_3$ composite coatings on mild steel

Additive/Constituent	**Mass concentration (g/L)**
$ZnSO_4{\cdot}7H_2O$	143.80
Na_2SO_4	49.71
H_3BO_3	30.92
$SC(NH_2)_2$	10
$C_6H_{12}O_6$	5

The mass blend mix of PS-$CaCO_3$ to ES-$CaCO_3$ in the bath was varied in the following ratios: 1:0 (4.56 g PS + 0 g ES); 0.5:0.5 (2.28 g PS + 2.28 g ES); 0.3:0.7 (1.37 g PS + 3.19 g ES); 0.1:0.9 (0.46 g PS + 4.10 g ES); and 0:1 (0 g PS + 4.56 g ES); for corrosion performance evaluation. A-dual zinc anode setup was used under controlled time and stirring, while incorporating nano-$CaCO_3$ PS and ES particles into the bath. ZnO mass

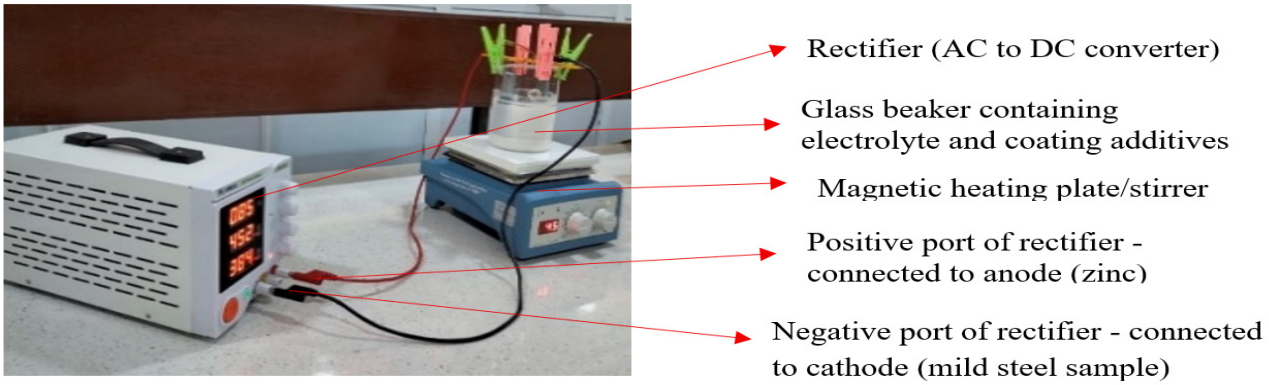

Figure 1: Setup for electrolytic deposition of Zn and Zn-ZnO-$CaCO_3$ composite coatings on mild steel

was constant at 3.5 g in every 350 mL Zn sulphate electrolyte volume used. Image of the setup used for the electrolytic deposition of Zn and the bi-layer composite coatings on mild steel is presented in Fig. 1.

The image in Fig. 1 was captured using an OPPO A53s mobile device (Model: CPH2135) featuring a triple-rear end camera system with 13 Megapixels (Sensor Model: OV13B), f/2.2 aperture, and a 5-Piece lens.

3. Coating thickness measurements and corrosion tests

3.1. Thickness of Zn and Zn/Zn-ZnO-$CaCO_3$ composite coatings electrodeposited on mild steel

Thickness measurements of Zn and Zn/Zn-ZnO-$CaCO_3$ composite coatings on mild steel were carried out with Elcometer® 456/4 Dry Film Thickness Guage (Serial number: ZC32826), using an F1 Probe Type (Serial number: ZF11851). The analysis of the thickness data was done using Elcomaster® 2.0.81 Software.

3.2. Electrochemical kinetic parameters of uncoated and bi-layered Zn/Zn-ZnO - $CaCO_3$ composite coated mild steel obtained in seawater by EFM

Electrochemical kinetic parameters of corrosion current (i_{corr}), oxidation/anodic reaction rate (β_a), and reduction/cathodic reaction rate (β_c) were all obtained for uncoated and bi-layered Zn/Zn-ZnO-$CaCO_3$ composite coated mild steel in seawater using EFM. EFM is a non-destructive electrochemical technique for measuring corrosion kinetics without prior knowledge of the Tafel coefficients. EFM also uses an integrated validity check called "causality factors." The causality factors (CF-2 and CF-3), show the relationship between the perturbation signal (frequency) and the output (current response); which primarily indicate uniform corrosion. Deviations of CF-2 and CF-3 from their expected theoretical values of 2 and 3 often signal influence of electrochemical noise or interference on the current response (Han & Song, 2008; Khaled, 2009; Amin et al., 2009).

The uncoated mild steel (control) and Zn/Zn-ZnO-$CaCO_3$ composite coated specimens were embedded in epoxy resin, exposing a surface area of ≈3.42 cm^2 (1.9 cm × 1.8 cm) in each case. Specimens were soaked in the seawater for one hour before each EFM measurement. EFM was performed at a base frequency of 1 Hz using potential perturbation frequencies of 2 and 5 Hz at 10 mV amplitude and 16 cycles for approx. 17 s. Gamry Instruments Potentiostat/Galvanostat/ZRA 11239 (Interface 1000^T) with Echem Analyst™ Software attached was used to analyze all electrochemical corrosion data. Subsurface seawater sample collected from NDL graven dockyard was the electrolyte used in the electrochemical corrosion studies. Fig. 2 (a) shows image of a Zn/Zn-ZnO-$CaCO_3$ composite coated mild steel, and (b) presents image of the uncoated and composite coated specimens mounted in epoxy resin to facilitate EFM corrosion measurements. These images were captured using the same device described in Section 2.2 of this report.

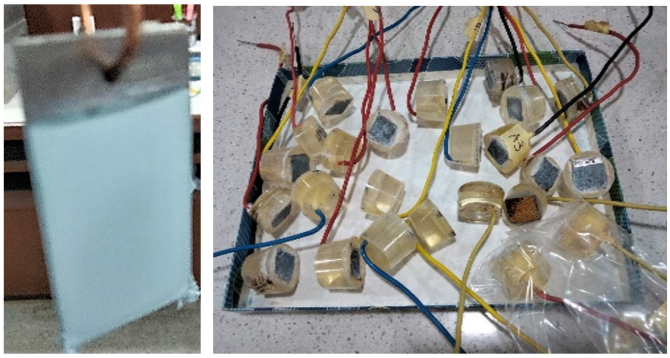

Figure 2: (a) Picture of a Zn/Zn-ZnO-$CaCO_3$ composite coated specimen, (b) uncoated and composite coated specimens mounted in epoxy for EFM corrosion tests

However, during pilot investigations, polarisation resistance in seawater of single-layer zinc-coated mild steel (exposed surface area of 1 cm^2) was evaluated by potentiodynamic polarisation (PTDYN) electrochemical technique using a-250 mL volume flat corrosion cell (Princeton Applied Research K0235) and a three-electrode setup. Test pieces were held at open circuit for one hour before application of the perturbation potential from an initial potential of -0.3 V relative to the open circuit potential (OCP) to a final potential of +1 V relative to the reference electrode (standard calomel electrode, SCE), at a scan rate of 0.1 mV/s. Electrochemical kinetic parameters of equilibrium corrosion potential (E_{corr}), equilibrium corrosion current (i_{corr}), anodic Tafel coefficient (β_a), and cathodic Tafel coefficient (β_c) were obtained by Tafel Fit analysis. Nevertheless, in addition to its destructive nature, determination of electrochemical parameters using PTDYN typically involves several trial-and-error curve-fitting extrapolations and approximations. Reportedly, this approach may introduce systemic errors in corrosion

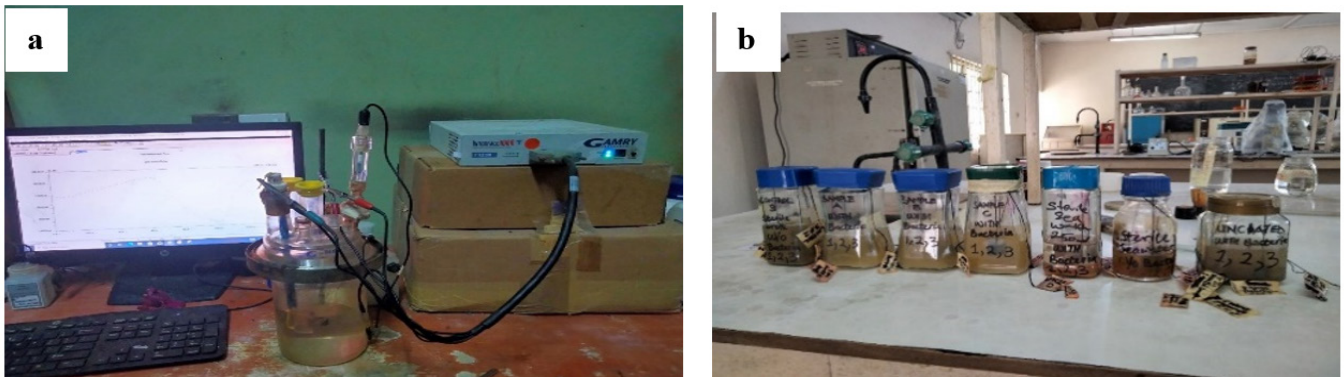

Figure 3: Image of laboratory setup used for: (a) EFM corrosion tests in seawater, and (b) MIC tests in SSW and SNB of uncoated and bi-layered Zn composite coated mild steel

measurements and/or interpretations (Abdel-Rehim et al., 2006; Obot & Onyeachu, 2018).

3.2.1. MIC of uncoated and bi-layered Zn/Zn-ZnO-$CaCO_3$ composite coated mild steel

MIC experiments were conducted on uncoated and Zn/Zn-ZnO-$CaCO_3$ composite coated mild steel. An automated-identified (VITEK 2 Systems, BioMérieux) sulphate-reducing bacteria (SRB) obtained from rust slurry of uncoated mild steel seawater exposures for 126 days was the organism for the MIC investigation. Mild steel specimens (triplicates) were subjected to sterile seawater (SSW) and sterile nutrient broth (SNB) exposures in the absence and presence of the SRB for 14 days for MIC tests. 13 g of the nutrient broth powder dissolved in 1000 mL distilled water had the following ingredients concentrations: peptone 5 g/L, meat extract # 1.5 g/L, yeast extract 1.5 g/L, and sodium chloride 5.0 g/L. pH of the nutrient broth was adjusted from 8.23 to 7.20 by adding drops of 1N NaOH (40 g of NaOH per litre of solution**)**. 1 L total volume of seawater and nutrient broth solutions each were autoclaved at 121 °C for 15 minutes and used for the MIC studies.

Bacterial load was adjusted to 0.5 MC Farland turbidity standard and 5 mL portion of the culture was inoculated into each 250 mL volume of SSW and SNB. The bio-flasks were vortexed and the sterilized specimens were immersed in the respective solutions. After 14 days exposures, bio-flasks with SRB inoculum were aseptically opened in the biosafety cabinet to retrieve the exposed mild steel specimens. To inactivate the bacterium upon retrieval, specimens were first immersed in 70 % ethanol, followed by sequential dipping in 50, 70, 80, 96, and 100 % ethanol solutions. Specimens' immersion in ethanol + acetic acid solution was followed by double rinsing in phosphate-buffered saline (PBS); and finally distilled water rinsing before drying under ambient laboratory air. The biofilms on two out of three specimens from the bio-flasks with SRB inoculum were removed; specimen surfaces were cleaned, and weights were measured. Weight measurements before and after 14 days were used to compute the weight change (ΔWt. g). The third specimen in each case was carefully preserved for surface analysis. Fig. 3 (a) shows image of the laboratory electrochemical corrosion setup used for EFM, and (b) shows the laboratory setup for MIC experiments. These images were captured using the same device described in Section 2.2.

3.3. SEM/EDS Characterization

Surface morphology and elemental compositional analysis were performed on selected coated and MIC tested coated mild steel using a Carl Zeiss Smart Evo Scanning Electron Microscope (SEM), manufactured by Carl Zeiss, Germany, with Energy Dispersion X-ray Spectroscope (EDS) attached at the Material Science and Engineering (MSE) Alumni Laboratories, Department of Materials Science and Engineering, Obafemi Awolowo University, Ile-Ife, Oyo State, Nigeria

3. Results and discussion

4.1. Chemical composition and microstructure of tested structural mild steel

Mild steel (shipbuilding grade) with chemical composition (wt.%) shown in Table 2 and optical microstructure presented in Fig. 4 was the study specimen.

4.1.2. Seawater physicochemical parameters

Some of the measured physicochemical parameters of the of the sterilized seawater (SSW) and nutrient broth (SNB) are shown in Table 3.

Table 2: Chemical composition (wt.%) of tested structural mild steel

Element	C	Si	Mn	P	S	Cr	Ni	Al	Cu	Nb	Fe
Wt. %	0.15	0.17	0.21	0.02	0.01	0.33	0.02	0.03	0.03	0.02	99.04

Table 3: Some physicochemical parameters of SSW and SNB used for MIC tests

Media	Oxidation Reduction Potential (mV)	Conductivity (mS/cm)	Dissolved Oxygen (mg/L)	Total Dissolved Solids (g/L)	Salinity (ppt)
SSW	+306	33.4	9.89	27.8	29.54
SNB	+188	7.73	10.33	4.87	4.26

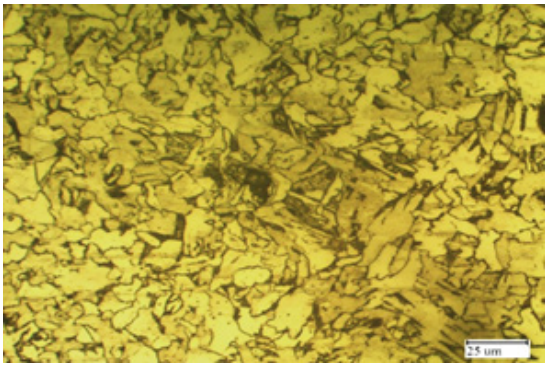

Figure 4: Optical microstructure (400*X*) of tested structural mild steel (as-received)

The measured pH of the seawater was 8.43. Oxidation-Reduction Potential (ORP) – electron transfer capacity, shows the oxidizing or reducing state of the seawater sample; where positive ORP values between +100 and +350 indicate oxic environments, where oxygen acts as a strong electron acceptor. Hence, the +306 ORP value of seawater shows a stronger oxidizing environment. Conductivity is a measure of the ionic content of the seawater; dissolved oxygen (DO) is the non-compound oxygen gas (O_2) available for aquatic life in the water. Total dissolved solids (g/L) indicate the total amount of inorganic and organic matter (salts, minerals, metals) dissolved in the solution (quantified as mass concentration in the volume tested); and salinity gives the number of dissolved salts measured in parts per thousand (ppt). Salinity is an important seawater (water) parameter because it determines the conductivity and general chemistry of the water. The SSW values were significantly higher than those of the SNB except in the DO case.

4.2. Central composite design of Zn-ZnO-$CaCO_3$ composite coatings on Zn-coated mild steel

The CCD randomized study for the Zn-ZnO-$CaCO_3$ electrolytic co-deposition on Zn-coated mild steel and the response results is shown in Table 4.

Table 4: CCD for Zn-ZnO-$CaCO_3$ electrolytic co-deposition on Zn-coated mild steel

		Factor 1	Factor 2	Factor 3	Response
Std	Run	(A): Current Density (A/cm^2)	(B): $CaCO_3$ mass conc. (g/0.35 L)	(C): Time (mins)	**Coating mass deposited (g)**
16	1	0.03	3.42	45	0.36
7	2	0.02	4.56	60	0.55
9	3	0.0131821	3.42	45	0.25
13	4	0.03	3.42	19.7731	0.17
15	5	0.03	3.42	45	0.29
10	6	0.0468179	3.42	45	0.26
17	7	0.03	3.42	45	0.27
1	8	0.02	2.28	30	0.22
3	9	0.02	4.56	30	0.25
14	10	0.03	3.42	70.2269	0.51
6	11	0.04	2.28	60	0.40
12	12	0.03	5.33724	45	0.35
8	13	0.04	4.56	60	0.33
11	14	0.03	1.50276	45	0.23
2	15	0.04	2.28	30	0.15
4	16	0.04	4.56	30	0.29
5	17	0.02	2.28	60	0.44

Table 5: Average Coating Thickness of Zn and Zn/Zn-ZnO-$CaCO_3$ composite coatings electrodeposited on mild steel

Specimen Tag	Coating Composition ($CaCO_3$ g - PS/ES)	Average Coating Thickness (µm)
Zn	-	68.65 ± 9.34
A	(Zn/Zn-ZnO-$CaCO_3$-4.56 g-PS)	88.82 ± 5.53
B	(Zn/Zn-ZnO-$CaCO_3$-2.28 + 2.28 g - PS+ES)	89.92 ± 2.28
C	(Zn/Zn-ZnO-$CaCO_3$-1.37 + 3.19 g – PS+ES)	92.10 ± 2.49
D	(Zn/Zn-ZnO-$CaCO_3$-0.46 + 4.10 g – PS+ES)	92.49 ± 7.73
E	(Zn/Zn-ZnO-$CaCO_3$-4.56 g-ES)	96.87 ± 4.8

Process optimization goals were set to maximize $CaCO_3$ mass concentration (Factor B) in the bath for the Zn-ZnO-$CaCO_3$ composite coating on Zn-coated mild steel, while keeping other factors (A and C) in range. A two-factor interaction (2FI) regression model as presented in Equation (1) was developed to predict mass of coating (Zn-ZnO-$CaCO_3$) deposited:

$$Mass\ of\ coating\ deposited = +0.2964 + 0.0006\,\boldsymbol{A} + 0.0329\,\boldsymbol{B} + 0.1039\,\boldsymbol{C} - 0.0134\,\boldsymbol{AB} - 0.0334\,\boldsymbol{AC} - 0.0514\,\boldsymbol{BC} \quad (1)$$

The analysis of variance (ANOVA) showed that the model significantly predicted the response variable with coefficient of determination, R^2 = 0.9787 (≈0.98), and p-value < 0.0010. $CaCO_3$ mass conc. (B) (p-value < 0.0457) and Time (C) (p-value < 0.0001) were significant model factors influencing the response. R^2 value, implies that 98% of the observed response results can be interpreted by the model, showing a close fit between the empirical and predicted data. Statistical significance of the model's predictive ability was substantiated by the Predicted vs. Actual plot presented in Fig. 5.

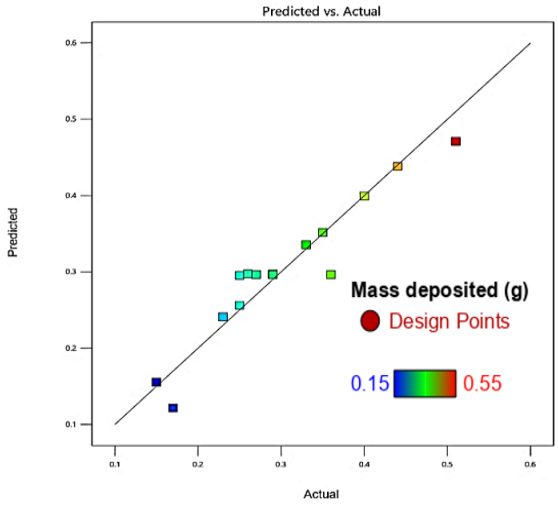

Figure 5: Predicted vs. Actual plot of 2FI model for Zn-ZnO-$CaCO_3$ coatings co-deposition

This plot shows the actual response results from the experiment against the model's predicted values. The good fit indicated by the high R^2 value can be visualized by the clustering of the points close to the regression line.

4.2.1. Thickness of Zn and Zn/Zn-ZnO-$CaCO_3$ composite coatings electrodeposited on mild steel

For every triplicate coating electrodeposition set, ten spots on either side of the coated mild steel specimen were measured and the average was software-computed. The average thickness of the coatings is shown in Table 5 with standard deviations.

The Zn/Zn-ZnO-$CaCO_3$-4.56 g-ES coated sample having 96.87 µm thickness, had a-28.22 µm increased thickness corresponding to 41.11 % increase in coating thickness over the Zn-coated mild steel.

4.2. Electrochemical Corrosion of bi-layered Zn/Zn-ZnO-$CaCO_3$ composite coatings on mild steel in seawater evaluated by EFM

EFM intermodulation spectra were obtained for uncoated and bi-layered Zn/Zn-ZnO-$CaCO_3$ composite coated mild steel in subsurface seawater. Fig. 6 (a) to (f) are examples representing the EFM intermodulation spectra obtained by Fast Fourier Transform (FFT) for six test specimens' sets.

Each EFM intermodulation spectrum is a plot of current (A) response as a function of frequency (Hz). The highest peaks (amplitudes) in the spectrum indicate the current response at the excitation frequencies of 2 and 5 Hz, but the lower peaks represent the harmonics, sums, and differences of the excitation frequencies. Examining Fig. 7 (a) to (f), the amplitudes of the current (A) at the two peak frequencies of 2 and 5 Hz is between: 10.00 and 130.00 µA (1×10^{-6}) for the intermodulation spectrum of the uncoated mild steel (a); 1.00 and 10.00 µA (1×10^{-6}) for intermodulation spectra of Zn/Zn-ZnO-$CaCO_3$ (4.56 g-PS-$CaCO_3$) composite coated and the blended (4.56 g-PS+ES-$CaCO_3$) composite coated mild steel. However, inspecting the intermodulation spectrum of the Zn/Zn-ZnO-$CaCO_3$ (4.56 g-ES-$CaCO_3$) coated mild steel, the current response amplitude at 2 and 5 Hz is

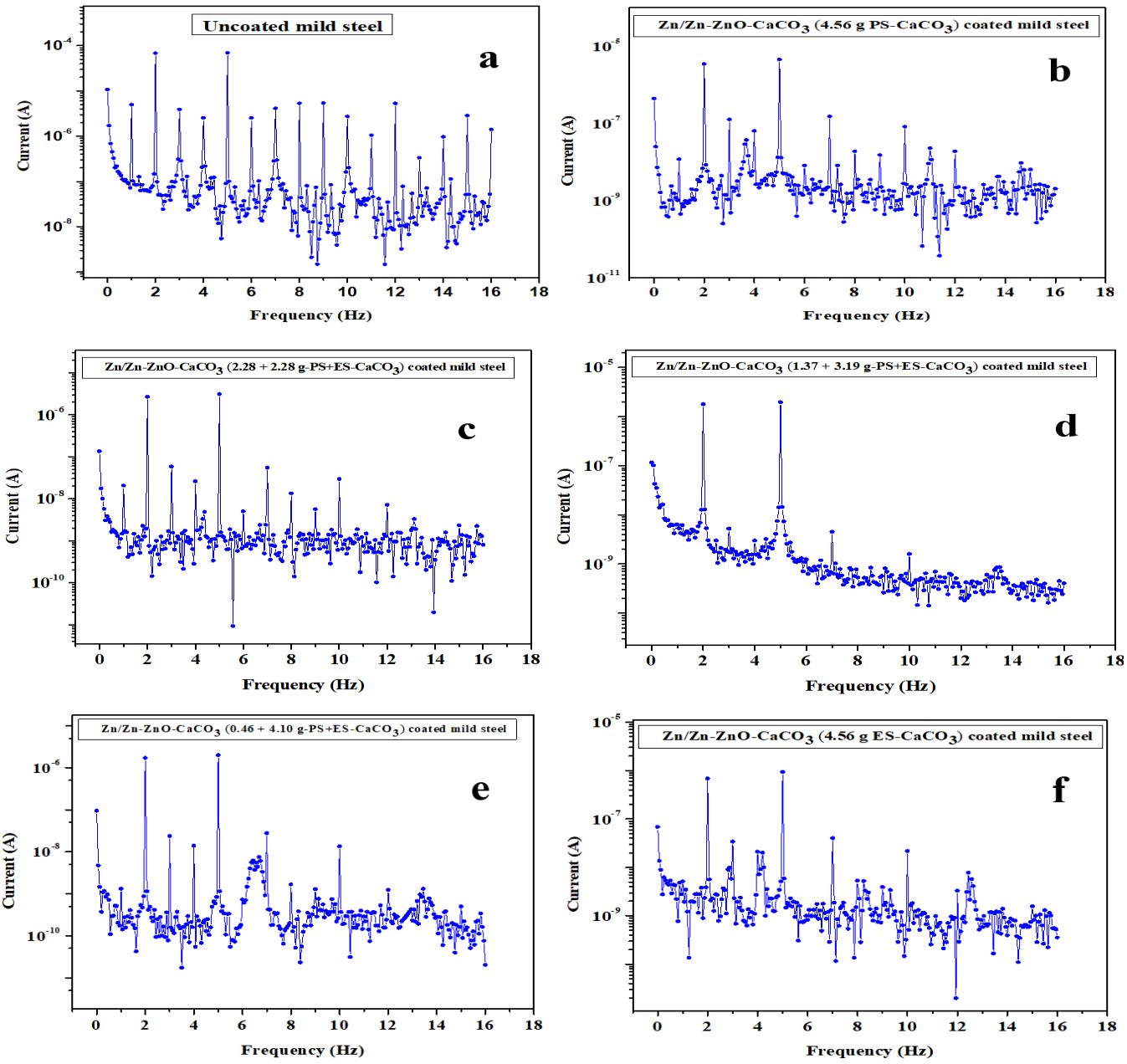

Figure 6: Current response intermodulation spectrum obtained with EFM for mild steel in seawater: (a) uncoated (UNCT); (b) Zn/Zn-ZnO-$CaCO_3$ (4.56 g-PS-$CaCO_3$) coated (A); (c) Zn/Zn-ZnO-$CaCO_3$ (2.28 + 2.28 g–PS+ES-$CaCO_3$) coated (B); (d) Zn/Zn-ZnO-$CaCO_3$ (1.37 + 3.19 g PS+ES) coated (C); (e) Zn/Zn-ZnO-$CaCO_3$ (0.46 + 4.10 g PS+ES) coated (D); (f) Zn/Zn-ZnO-$CaCO_3$ (4.56 g-ES-$CaCO_3$) coated (E) mild steel

between 100.00 nA (1×10^{-7}) and 1.00 µA (1×10^{-6}). The scale of the current axis is expressed using standard scientific notation. Notably, in EFM, the resulting non-linear current response (current amplitude) at the excitation frequencies defines polarisation resistance and, hence, the corrosion rate. Therefore, the lower the current (A), the higher the corrosion resistance at the electrode surface.

EFM measures the system's corrosion current (i_{corr}) as a non-liner response to the potential perturbation. The current responses at the peaks are used by EFM140™ Software to compute the electrochemical kinetic parameters in situ (Khaled, 2009). Table 6 presents the electrochemical kinetic parameters (i_{corr}, βa, βc, CF-2, and CF-3) obtained by EFM for 18 (6 × 3) mild steel empirical specimens in seawater electrolyte.

The corrosion mechanism can be obtained by analyzing the reaction rates of the specific chemical steps - oxidation (anodic) and reduction (cathodic) reactions, βa and βc (Tafel coefficients/constants/slopes.

Table 6: Electrochemical kinetic parameters obtained for uncoated and Zn/Zn-ZnO-$CaCO_3$ coated mild steel in seawater using EFM technique (Active corrosion analysis)

Specimen Tag/ Coating Composition (g $CaCO_3$)	S/N	i_{corr} (µA)	βa (10^{-3} V/ dec)	βc (10^{-3} V/dec)	CF-2	CF-3
UNCT	1	30.67	22.45	26.03	1.874	3.187
	2	30.29	20.68	26.87	1.679	2.935
	3	30.37	24.07	28.34	1.952	2.572
A (Zn/Zn-ZnO-$CaCO_3$-4.56 g PS)	1	12.08	161.5	240.1	1.743	2.865
	2	11.45	157.1	239.7	1.814	2.687
	3	11.90	159.5	242.1	2.318	3.230
B (Zn/Zn-ZnO-$CaCO_3$-2.28 + 2.28 g - PS+ES)	1	8.53	157.7	215.8	1.971	3.132
	2	7.85	159.7	198.2	2.013	2.952
	3	8.19	166.0	207.5	2.039	3.178
C (Zn/Zn-ZnO-$CaCO_3$-1.37 + 3.19 g – PS+ES)	1	10.51	354.5	376.2	2.018	3.173
	2	10.39	351.7	373.4	2.351	2.758
	3	10.56	357.8	379.5	1.527	3.712
D (Zn/Zn-ZnO-$CaCO_3$-0.46 + 4.10 g – PS+ES)	1	12.87	380.6	552.4	1.894	3.321
	2	12.26	360.9	532.7	2.112	3.462
	3	12.66	375.4	546.9	1.882	2.752
E (Zn/Zn-ZnO-$CaCO_3$-4.56 g ES)	1	2.03	130.3	214.9	1.909	2.730
	2	2.10	133.2	225.4	1.922	2.590
	3	2.12	136.9	221.7	2.269	2.924

In electrochemical corrosion science, a low value of βa suggests a simple rapid charge-transfer reaction mechanism (charge-transfer controlled kinetics). In contrast, a high value of βc typically indicates a complex, multi-step electron transfer process or presence of an insulating film (Wang, 2025). Moreover, in the context of chemical kinetics, the slowest step in the sequence of a multi-step reaction process, is the rate-determining step (RDS), which controls the reaction mechanism. Inspecting Table 6, oxidation reaction rates (βa) were consistently slower (lower values) than the reduction reaction rates (βc). This observation strongly suggests that the electrochemical kinetics of the uncoated and coated mild steel in the seawater marine environment follows activation-controlled corrosion - the controlling mechanism is active corrosion mechanism. Therefore, the speed of the corrosion process in the seawater is limited by electron transfer/charge transfer kinetics. This means that the overall reaction rate is limited by "how fast" metallic atoms can leave the metal lattice to enter the seawater solution as ions. Notably, faster reduction reaction rates observed for the bi-layered composite coatings indicate efficient barrier and highly catalytic interfaces (Wei et al., 2025).

Furthermore, the causality factors (CF-2 and CF-3) as-observed were close to their theoretical values of 2 and 3, indicating high quality of the measured data, which validates the mathematical relationship between the kinetic parameters and active corrosion mechanism (Han & Song, 2008; Amin et al., 2009). Using the corrosion current (i_{corr}, µA) obtained, corrosion current density (j_{corr}, µA/cm^2) was calculated; and corrosion rate (*CR*, mm/yr) was calculated from j_{corr} as penetration rate using the expression (Amin et al., 2009):

$$CR\ (\text{mm/yr}) = 0.00327 \times j_{corr} \times \frac{M}{n\rho} \quad (2)$$

Where, *CR* is the corrosion rate in millimeter per year (mm/yr), 0.00327 a conversion constant, j_{corr} the corrosion current density (µA/cm^2), *M* the atomic weight of iron (Fe = 55.85g), *n* number of electrons transferred during the oxidation of one atom of Fe (n = 2), and ρ the density of Fe (7.87 g/cm^3). Normalised polarisation resistance, *Rp*, (**Ω**.cm^2) was determined using the Stern-Geary equation (Han &Song, 2008) presented in Equation 3:

$$Rp = \frac{\beta a \beta c}{2.303 \times j_{corr} \times (\beta a + \beta c)} \quad \text{(Active corrosion)} \quad (3)$$

Where, βa and βc are the oxidation and reduction reaction rates in volts per current decade (V/dec), and j_{corr} the corrosion current density (A/cm^2). Corrosion protection efficiency, E_{EFM} (%) (Khaled, 2009), of the bi-layered composite coatings was evaluated using the following relation:

$$E_{EFM}\% = 1 - \frac{j_{corr}}{j^{\circ}_{corr}} \times 100 \quad [4]$$

Where, j_{corr} and j°_{corr} are the corrosion current densities (µA/cm^2**)** of the coated and uncoated mild steel respectively. Average i_{corr} (µA) using two and/or three concordant measurements - with difference of not more than ± 0.5 (see Table 7) was computed as mean showing

Table 7: Average EFM corrosion current, current density, corrosion rate, polarisation resistance, and coating efficiency

Specimen Tag	i_{corr} (µA)	j_{corr} (µA/cm²)	*CR* (mm/yr)	*Rp* (Ω.cm²)	E_{EFM} (%)
UNCT	30.44 ± 0.16	8.90	0.10	597.66	N/A
A	11.81 ± 0.26	3.45	0.04	12058.66	61.24
B	8.19 ± 0.28	2.39	0.04	16424.84	73.15
C	10.49 ± 0.07	3.07	0.03	25857.22	65.51
D	12.60 ± 0.25	3.68	0.04	26056.68	58.65
E	2.08 ± 0.04	0.61	0.007	59260.17	93.15

standard deviations. Table 7 presents average i_{corr}, j_{corr}, *CR*, *Rp*, and E_{EFM} calculated using EFM kinetic data obtained.

From Table 7, the uncoated mild steel (UNCT) showed the highest *CR* at 0.10 mm/yr; Sample E (Zn/Zn-ZnO-4.56 g ES-derived $CaCO_3$) displayed the lowest *CR* at 0.007 (7.05×10^{-3}) mm/yr. *Rp* of UNCT was the observed lowest at 597.66 Ω.cm²; however, the largely ES-4.56 g $CaCO_3$ (coating E) displayed the highest *Rp* at 59,260.17 Ω.cm². Thus, presenting 98.15% improvement in *Rp* relative to the uncoated mild steel. Notably, considerable reductions in *CR* (from 0.10 to 0.04 and 0.03 mm/yr) were observed in the PS-$CaCO_3$, and PS+ES-$CaCO_3$ blended composite coatings (A to D). As observed, the composite coating containing optimal mass concentration of 4.56 g ES-$CaCO_3$ displayed the highest corrosion protection efficiency, E_{EFM} (%), of all tested bi-layered composite coatings at 93.15%. XRD confirmed the dominant mineral phase in the ES-$CaCO_3$ as calcite and that of PS-$CaCO_3$ as predominantly aragonite (Nnaji et al., 2023). The significant improvement in corrosion performance of the Zn/Zn-ZnO-4.56 g-ES-$CaCO_3$ composite coating - Specimen E (low *CR* and high *Rp*) is attributable to the high purity of the electrodeposition raw materials, controlled and optimised coating conditions, higher coating thickness as well as the higher stability of calcite-dominant ES-$CaCO_3$ in subsurface seawater. It is suggested that the metastability and higher solubility of aragonite under subsurface seawater conditions (Sulpis et al., 2022) influenced the reduced *Rp* of the PS-$CaCO_3$-containing coatings.

Polarisation curves recorded using PTDYN for Zn-coated mild steel in seawater during earlier corrosion studies are shown in Fig. 7, and electrochemical kinetic parameters obtained by Tafel Fitting are presented in Table 8.

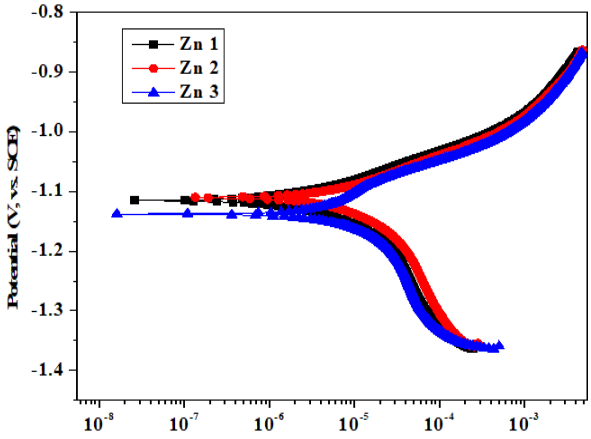

Figure 7: Polarisation curves obtained for Zn-coated mild steel in seawater

CR and *Rp* were estimated using Equations (2) and (3) presented earlier. From Table 8, the higher *βc* values relative to *βa* also indicate active corrosion mechanism of the single-layer Zn coating on mild steel. Average *CR* of Zn coating at 0.06 mm/yr had a corresponding average *Rp* of 2896.66 Ω.cm². The *Rp* values of all tested specimens' sets arranged from lowest to highest follow the sequence: UNCT < Zn < A < B < C < D < E.

Generally, the bi-layered Zn/Zn-ZnO-$CaCO_3$ composite coatings displayed higher corrosion resistance than the single-layer Zn coating. However, the 4.56 g ES nano-$CaCO_3$ modified bi-layered composite coating out-performed the PS + ES blend mix nano-$CaCO_3$ modified bi-layered coatings. The superior anti-corrosion properties demonstrated by the ES nano-$CaCO_3$-modified composite coating is consistent with Aigbodion and Onuoha (2024). In comparison with earlier research results on single-layer Zn, Zn-$CaCO_3$,

Table 8: Electrochemical Kinetic Parameters obtained for Zn-coated Mild Steel in seawater

S/N	E_{corr} (V)	i_{corr} (µA)	*βa* (10^{-3} V/dec)	*βc* (10^{-3} V/dec)	*CR* (mm/yr)	*Rp* (Ω.cm²)
Zn 1	-1.11	6.26	60.4	95.7	0.07	2568.49
Zn 2	-1.12	5.53	56.3	89.3	0.06	2711.31
Zn 3	-1.14	5.36	80.2	88.6	0.06	3410.18

Table 9: MIC rate of uncoated and coated mild steel exposed to *P. mirabilis* in SSW and SNB

S/N	Bio flask Description	**Specimen Coating Description**	ΔWt. (g)	***CR* (mm/yr)**
1	SSW W/O *P. mirabilis*	Uncoated	0.02	0.03
2	SNB W/O *P. mirabilis*	Uncoated	0	0
3	SSW with *P. mirabilis*	Uncoated	0.08	0.11
4	SNB with *P. mirabilis*	Uncoated	0.02	0.03
5	SSW with *P. mirabilis*	Zn/Zn-ZnO-$CaCO_3$(4.56 g PS)	0	0
6	SNB with *P. mirabilis*	Zn/Zn-ZnO-$CaCO_3$(2.28 g + 2.28 g-PS/ES)	0	0
7	SSW with *P. mirabilis*	Zn/Zn-ZnO-$CaCO_3$(4.56 g ES)	0	0

and Zn-eggshell particle composite coatings on mild steel corrosion (Fardilah et al., 2025; Aigbodion & Akinlabi, 2019); the findings of this study investigation demonstrated a lower corrosion rate (0.007 < 0.027 mm/yr) and higher polarisation resistance (17,327.54 > 9691 Ω) – unnormalised (raw) *Rp* of the 4.56 g ES nano-$CaCO_3$-modified bi-layered Zn/Zn-ZnO-$CaCO_3$ composite coating – while elucidating the fundamental corrosion mechanism of the coated and uncoated mild steel in seawater marine environment.

4.2.1. MIC of uncoated and bi-layered Zn/Zn-ZnO-$CaCO_3$ composite coatings in SSW and SNB

Proteus mirabilis (*P. mirabilis*) was identified from the rust slurry microbial analyses to a-99 % presence using Vitek 2 machine-strip (sixty-four (64) biochemicals). MIC rate of uncoated and Zn/Zn-ZnO-coated mild steel was evaluated using weight loss measurements after 14 days exposures to SSW and SNB in the presence of *P. mirabilis*. MIC rate was evaluated according to ASTM G31 standard using Equation 5:

$$CR\ (mm/yr) = \frac{K \times W}{A \times t \times \rho} \quad (5)$$

Where, *K* is a conversion constant (8.76×10^4), *W* is mass loss (g), *A* is exposed surface area (22.8 cm^2), *t* is time (hours), and ρ is density (g/cm^3). Average weight loss (*ΔWt.*) and MIC rate *(CR*) calculated from 3 replicate measurements is presented in Table 9.

CR of uncoated mild steel in sterile seawater in the presence of *P. mirabilis* (SSW with *P. mirabilis* – bio flask 3) at 0.11 mm/yr was approximately four (4) times more than its *CR* in sterile seawater in the absence of *P. mirabilis* (bio flask 1) as well as its *CR* in sterile nutrient broth with *P. mirabilis* (bio flask 4). No mass changes were observed in the Zn/Zn-ZnO-$CaCO_3$ coated mild steel specimens (bio flasks 5 to 7). Generally, the uncoated mild steel experienced more dissolution *in* SSW than in SNB solution in the presence of *P. mirabilis.* It is suggested that the seawater environment conditions, especially, ORP, conductivity, TDS, and salinity aided the higher corrosion rate of the mild steel under the SRB biofilm.

4.3 Surface investigation of uncoated and bi-layered coated mild steel by SEM/EDS

Surface morphology and composition of uncoated, selected Zn/Zn-ZnO-$CaCO_3$ coated, and corrosion tested mild steel examined using SEM/EDS are presented in Figs. 8 to 12.

Scanning electron micrograph of the Zn/Zn-ZnO-$CaCO_3$ - PS-4.56 g composite coated mild steel surface showed a textured acicular morphology; in contrast, the surface of ES-$CaCO_3$ (4.56 g) composite coated mild steel showed a dense and compact morphology. EDS

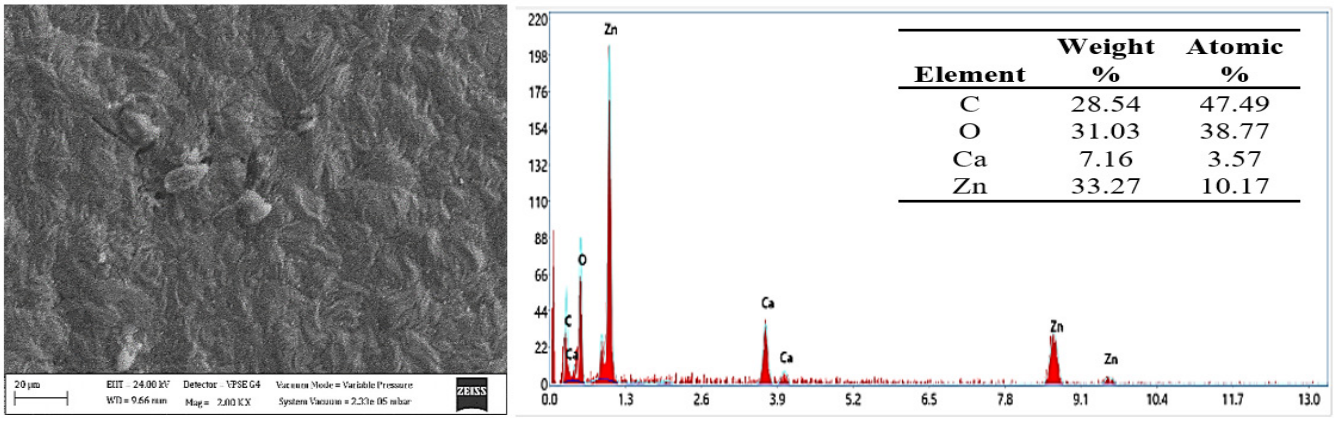

Element	Weight %	Atomic %
C	28.54	47.49
O	31.03	38.77
Ca	7.16	3.57
Zn	33.27	10.17

Figure 8: (a) Scanning electron micrograph of Zn/Zn-ZnO-$CaCO_3$ (4.56 g PS) composite coating on mild steel specimen, (b) EDS spectrum

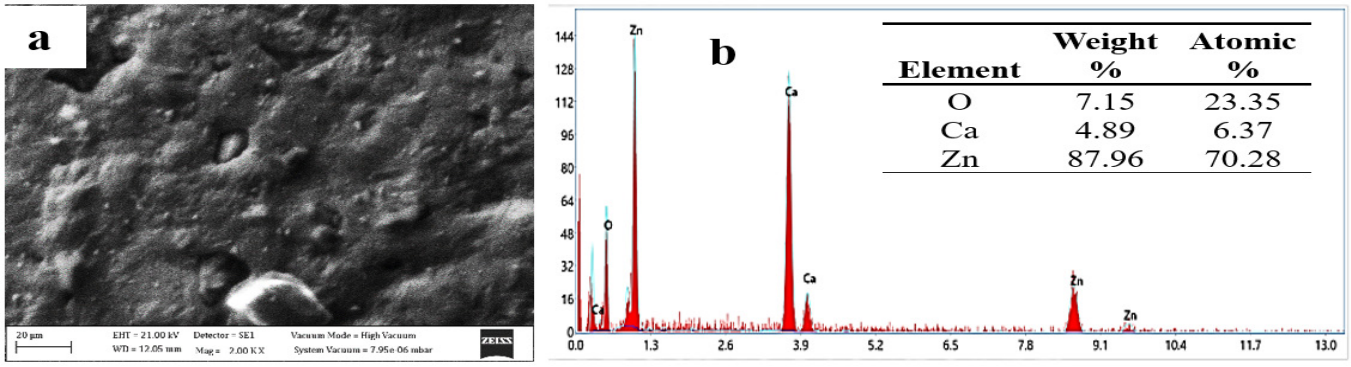

Figure 9: (a) Scanning electron micrograph of Zn/Zn-ZnO-$CaCO_3$ (4.56 g ES) composite coating on mild steel specimen, (b) EDS spectrum

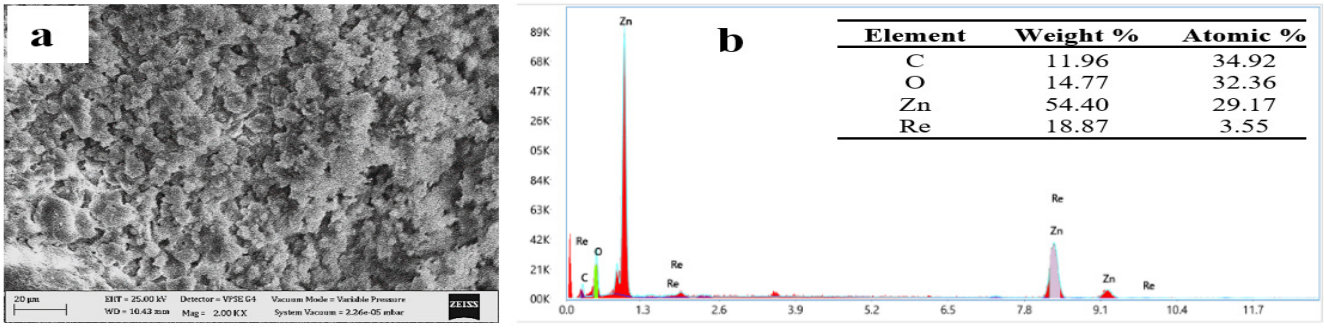

Figure 10: (a) Scanning electron micrograph of a Zn/Zn-ZnO-$CaCO_3$ (4.56 g PS) coated mild steel surface after14 days exposure to *P. mirabilis* culture in SSW, (b) EDS spectrum

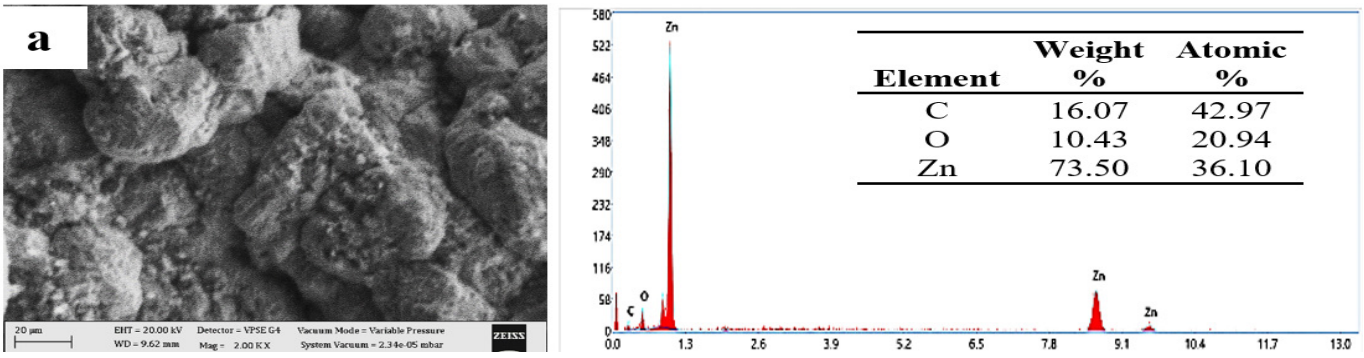

Figure 11: (a) Scanning electron micrograph of a Zn/Zn-ZnO-$CaCO_3$ (4.56 g ES) coated mild steel surface after14 days exposure to *P. mirabilis* culture in SSW, (b) EDS spectrum

confirmed presence of carbon (C), oxygen (O), calcium (Ca), and zinc (Zn) in the $CaCO_3$ modified composite coatings. Normalizing the EDS atomic % values using the least abundant element (Ca = 3.57), empirical ratios can be derived for the metallic elements (Ca and Zn) and the light-elements (C and O) as follows: in the 4.56 g PS-$CaCO_3$ reinforced composite coating, C = 13.30, O = 10.86 (≈ 11), Ca = 1.00, Zn = 2.85 (≈ 3); in the 4.56 g ES-$CaCO_3$ reinforced composite coating, O = 3.67, Ca = 1.00, Zn = 11.03 (≈ 11). Hence, the metal-to-metal (Ca-to-Zn) ratio in the PS-$CaCO_3$ composite coating is 1:3, suggesting a theoretical $CaZn_3$ metal framework; the Ca-to-Zn ratio in the ES-$CaCO_3$ composite coating will be 1:11, suggesting a $CaZn_{11}$ intermetallic phase. However, the significant surface atoms of C (47.49%) and O (38.77%) observed in the PS-$CaCO_3$ composite coating relative to the total metallic atoms (Ca + Zn = 13.74), further suggests a "mixed Zn-$CaCO_3$" phase. The 76.65% (Ca + Zn) metal atoms with substantial oxygen atoms (23.35%) observed in the ES-$CaCO_3$ composite coating additionally hints at a "metal-rich composite system, where the $CaZn_{11}$ is embedded in an oxide layer or oxide matrix. It is worthy to note that clear differences exist in the chemical, physical, thermodynamic and structural properties of various Ca_xZn_x intermetallic

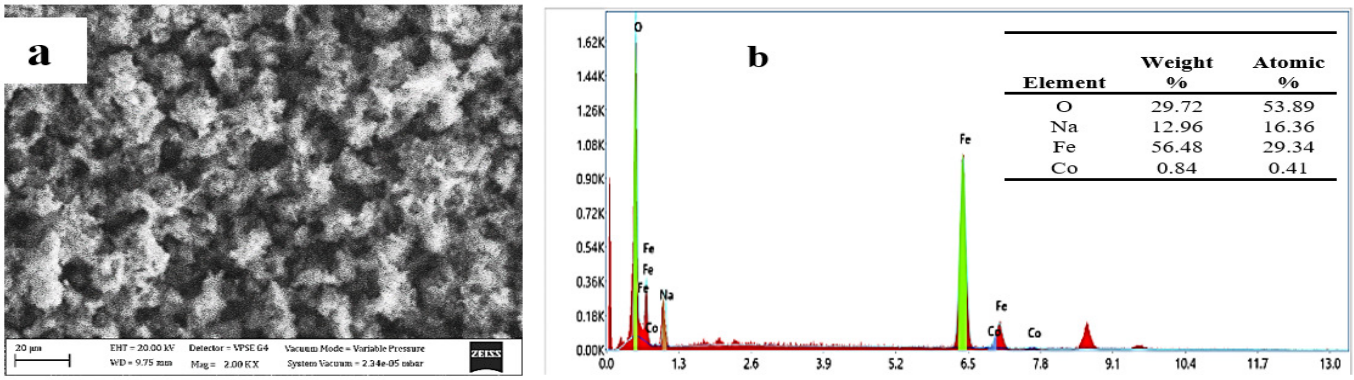

Figure 12: (a) Scanning electron micrograph of uncoated mild steel surface after14 days exposure to *P. mirabilis* culture in SSW, (b) EDS spectrum

compounds in Ca-Zn composite systems (Yang et al., 2012; Wang et al., 2024).

After 14 days exposure to *P. Mirabilis* in SSW, Zn/Zn-ZnO-$CaCO_3$ - PS-4.56 g coated mild steel surface displayed a flocculent biofilm and EDS revealed presence of C, O, Zn, and rhenium (Re). Though unconfirmed, it was suggested that the presence of Re possibly originated from the seawater solution. Surface of the Zn/Zn-ZnO-$CaCO_3$ - ES-4.56 g composite coated mild steel exposed to *P. Mirabilis* for 14 days in SSW showed sludge-like biofilm deposits; with EDS elemental composition showing C, O, and Zn. On the other hand, the uncoated mild steel specimen exposed to *P. mirabilis* in SSW for 14 days displayed porous mushy biofilm deposits. EDS elemental composition indicated high atomic % of oxygen at 53.89%, iron (Fe) at 29.34%, and sodium (Na) at 16.36%. Ignoring the minor atomic presence of cobalt (Co) at 0.41%, an estimation of molar ratios of Na:Fe:O yields approximately 1:1:6. Within the context of stable oxidation states and chemical stoichiometry, the existence of "$NaFeO_6$" as a compound is not feasible. However, the calculated theoretical stoichiometric ratios suggest presence of a complex ion and/or compound corrosion product of the uncoated mild steel in the seawater solution.

4. Conclusion and recommendations

5.1. Conclusion

In this research, $CaCO_3$ synthesized from biogenic wastes of periwinkle shell and chicken eggshell were successfully utilised in the fabrication of bi-layered Zn/Zn-ZnO-$CaCO_3$ composite coatings on structural mild steel via electrolytic co-deposition route.

The results of this investigation lead to the following conclusions:

1. Coefficient of determination, R^2 (≈0.98), ANOVA p-value (0.0010), and predicted vs. actual plots of developed regression model for Zn-ZnO-$CaCO_3$ composite co-deposition on Zn-coated mild steel validate its statistical relevance and predictive ability at the established $CaCO_3$ mass concentration optimized settings.
2. Corrosion evaluation of bi-layered composite coatings by EFM gives insights into the corrosion mechanism and obtains kinetic parameters in situ.
3. Quantitative empirical EFM data establishes active corrosion as the controlling mechanism of single-layer Zn-coated, uncoated and bi-layer Zn/Zn-ZnO-$CaCO_3$ composite coated mild steel in seawater in real-time test exposures.
4. PS and ES derived $CaCO_3$ nanofillers in Zn-ZnO matrix bi-layer coating on pure Zn underlayer improve corrosion resistance of mild steel in seawater marine environment.
5. There is a progressive increase in *Rp* as ES-$CaCO_3$ mass increase to the optimal 4.56 g concentration in the best-performing bi-layer composite coating.
6. Bi-layered Zn/Zn-ZnO-$CaCO_3$ composite coatings suppressed MIC of mild steel in in S S W and SNB.
7. SEM reveals dense, compact, and smooth coating surface morphologies, and EDS confirms considerable wt.% of atomic Zn and Ca in the bi-layer composite coatings, with the Ca attributable to the PS and ES sources.

Moving beyond the conventional classification of Zn coatings as purely sacrificial, this study demonstrates tripartite mechanism: sacrificial protection from Zn, insulating barrier driven by ZnO, and $CaCO_3$, which

suppresses MIC triggered by accumulation of *Proteus mirabilis* biofilms. This study provides quantitative evidence – coating thickness ≈ 97 µm, $CR \approx 0.007$ mm/yr, $Rp \approx 59{,}260\ \Omega.cm^2$, and E_{EFM} coating efficiency ≈ 93%; that the calcite-dominant ES-modified bi-layered Zn/Zn-ZnO-$CaCO_3$ coating with optimized 4.56 g nano-$CaCO_3$ outperforms earlier investigations of electrodeposited single-layer zinc, Zn-$CaCO_3$ and Zn-eggshell particle composite coatings corrosion protection of mild steel in seawater marine environment. Thus, filling a clear knowledge gap in composition-property relationships. By mapping the oxidation (anodic) and reduction (cathodic) kinetic pathways from the EFM data, this research offers a deeper understanding of electrochemical corrosion mechanism and provides a novel mechanistic framework for bi-layered zinc composite architectures for marine engineering application.

5. Recommendations

Corrosion testing timeline should be extended beyond short-term immersion to investigate long-term corrosion kinetics by diffusion and passivation using continuous EFM and electrochemical noise (EN) for industry viability. The interfacial chemistry (mild steel/Zn coating/ Zn-ZnO-$CaCO_3$ composite coating) and corrosion products of the uncoated and bi-layer composite coated mild steel in seawater should be investigated to further validate marine corrosion mechanisms.

6. Acknowledgement

The authors deeply appreciate Mr. Kazeem Oluwafemi Orebiyi and Mrs. Adenike Ogunbodede of the Public Health and Environment Lab; Dr. Basheeru Kazeem Adebayo of Central Research and References Laboratories, all of The University of Lagos, Akoka, Nigeria for their immeasurable logistical support to the study. Special thanks to Ms. Ebele Victoria Onugha of the Quality Control Department of Dormanlong Engineering Limited, Lagos. We acknowledge Dr. Aremo of MSE Alumni Lab, Obafemi Awolowo University, Ile-Ife, Oyo State, Nigeria for his assistance with the SEM/EDS analysis.

7. Declaration of conflicting interest

The authors declare that they have no known conflicts of interests or personal relationships that could have influenced the work reported in this paper.

References

Abdel-Rehim, S. S., Khaled, K. F., & Abd-Elshafi, N. S. (2006) Electrochemical frequency modulation as a new technique for monitoring corrosion inhibition of iron in acid media by new thiourea derivative. *Electrochimica Acta*, 51(16), 3269-3277. doi: 10.1016/j.electacta.2005.09.018.

Aigbodion, V. S., & Akinlabi, E. T. (2019) Explicit microstructural evolution and electrochemical performance of zinc-eggshell particles composite coating on mild steel. *Surfaces and Interfaces*, 17, 100387. doi: 10.1016/j.surfin.2019.100387.

Aigbodion, V. S., & Dinneya-Onuoha, E. (2024) Unveiling the anti-corrosion properties of Zn-eggshell particle composite coatings on mild steel in seawater-simulated solution using starch as a modifier. *RSC advances*, 14(34), 24548-24560. doi: 10.1039/d4ra04283b

Amin, M. A., Abd El Rehim, S. S., & Abdel-Fatah, H. T. (2009) Electrochemical frequency modulation and inductively coupled plasma atomic emission spectroscopy methods for monitoring corrosion rates and inhibition of low alloy steel corrosion in HCl solutions and a test for validity of the Tafel extrapolation method. *Corrosion Science*, 51(4), 882-894. doi: 10.1016/j.corsci.2009.01.006.

Benea, L., Mardare, L., and Simionescu, N. (2018) Anticorrosion performances of modified polymeric coatings on E32 naval steel in sea water. *Progress in Organic Coatings,* 123, 120-127. doi:10.1016/j.porgcoat.2018.06.020.

Chohan, I. M., Ahmad, A., Sallih, N., Bheel, N., Salilew, W. M., & Almaliki, A. H. (2024) Effect of seawater salinity, pH, and temperature on external corrosion behavior and microhardness of offshore oil and gas pipeline: RSM modelling and optimization. *Scientific Reports*, 14(1), 16543. doi: 10.1038/s41598-024-67463-2.

de la Fuente, D., Díaz, I., Alcántara, J., Chico, B., Simancas, J., Llorente, I., ... & Morcillo, M. (2016) Corrosion mechanisms of mild steel in chloride-rich atmospheres. *Materials and Corrosion*, 67(3), 227-238. doi: 10.1002/maco.201508488.

Fardilah, V. A., Schmahl, W. W., Pusparizkita, Y. M., Aslan, C., Tauviqirrahman, M., Jamari, J., & Bayuseno, A. P. (2025) Electrodeposited Zn and Zn–CaCO3 composite on mild steel for biodiesel storage tanks: Corrosion resistance evaluation. *Results in Surfaces and Interfaces*, 18, 100426. doi: 10.1016/j.rsurfi.2025.100426.

Han, L., & Song, S. (2008). A measurement system based on electrochemical frequency modulation technique for monitoring the early corrosion of mild steel in seawater. *Corrosion Science*, *50*(6), 1551-1557. doi: 10.1016/j.corsci.2008.02.009.

Idora, M. N., Rahman, M. M., Ismail, M., & Mohd Norsani, W. N. W. (2014) Effect of zinc coating thickness on corrosion performance of mild steel in atmospheric and seawater environment. *Applied Mechanics and*

Materials, 554, 213-217. doi:10.4028/www.scientific.net/AMM.554.213.

Jia, R., Yang, D., Xu, J., Xu, D., & Gu, T. (2017) Microbiologically influenced corrosion of C1018 carbon steel by nitrate reducing Pseudomonas aeruginosa biofilm under organic carbon starvation. *Corrosion Science*, 127, 1-9. doi: 10.1016/j.corsci.2017.08.007.

Kamburova, K., Boshkova, N., Boshkov, N., & Radeva, T. S. (2021) Composite coatings with polymeric modified ZnO nanoparticles and nanocontainers with inhibitor for corrosion protection of low carbon steel. *Colloids and Surfaces A: Physicochemical and Engineering Aspects*, 609, 125741. doi: 10.1016/j.colsurfa.2020.125741.

Khaled, K. F. (2009) Evaluation of electrochemical frequency modulation as a new technique for monitoring corrosion and corrosion inhibition of carbon steel in perchloric acid using hydrazine carbodithioic acid derivatives. *Journal of applied electrochemistry*, *39*(3), 429-438. doi: 10.1007/s10800-008-9688-y.

Lamprakou, Z., Bi, H., Weinell, C. E., & Dam-Johansen, K. (2023) Encapsulated corrosion inhibitive pigment for smart epoxy coating development: an investigation of leaching behavior of inhibitive ions. *ACS omega*, 8(16), 14420-14429. doi: 10.1021/acsomega.2c07853.

Liao, J., Li, H., Zeng, W., Sauer, D. B., Belmares, R., & Jiang, Y. (2012). Structural insight into the ion-exchange mechanism of the sodium/calcium exchanger. *Science*, 335(6069), 686-690. doi: 10.1126/science.1215759.

Liu, S., Zhao, X., Zhao, H., Sun, H., & Chen, J. (2017) Corrosion performance of zinc coated steel in seawater environment. *Chinese journal of oceanology and limnology*, 35(2), 423-430. doi: 10.1007/s00343-016-5269-9.

Liu, X., Wang, Y., Song, Y., Liu, W., Zhang, J., Li, N., ... & Han, E. H. (2024) The respective roles of sulfate-reducing bacteria (SRB) and iron-oxidizing bacteria (IOB) in the mixed microbial corrosion process of carbon steel pipelines. *Corrosion Science*, 240, 112479. doi: 10.1016/j.corsci.2024.112479.

Liu, X., Zeng, B., & Lin, G. (2022) Arsenic (As) contamination in sediments from coastal areas of China. *Marine Pollution Bulletin*, 175, 113350. doi: 10.1016/j.marpolbul.2022.113350.

Margapuram, D., Salgues, M., Lami, R., Erable, B., Groc, M., Vuillemin, R., ... & Bertron, A. (2024) Short-term interactions of concrete, biofilm, and seawater in the submerged zone of marine environments for sustainable floating offshore wind turbines. *Construction and Building Materials*, 451, 138840. doi: 10.1016/j.conbuildmat.2024.138840.

Melchers, R. E. (2005) The effect of corrosion on the structural reliability of steel offshore structures. *Corrosion science*, *47*(10), 2391-2410. doi: 10.1016/j.corsci.2005.04.004.

Melchers, R. E. (2007) The effects of water pollution on the immersion corrosion of mild and low alloy steels. *Corrosion Science,* 49(8), 3149-3167. doi:10.1016/j.corsci.2007.03.021

Nnaji, R. N., Bodude, M. A., & Esezobor, D. E. (2023) Electrolytic Co-deposition of Zn-ZnO and Zn-ZnO-$CaCO_3$ Composite Substrates on Low-Carbon Steel. *Nigerian Journal of Technological Development*, 20(2). doi: 10.4314/njtd.v18i4.1314.

Obot, I. B., & Onyeachu, I. B. (2018) Electrochemical frequency modulation (EFM) technique: Theory and recent practical applications in corrosion research. *Journal of Molecular Liquids*, 249, 83-96. doi: 10.1016/j.molliq.2017.11.006.

Popoola, A. P. I.; Fayomi, O. S. I.; Aigbodion, V. S; Abdulwahab, M. (2016) Surface modification, strengthening effect and electrochemical comparative study of Zn-Al_2O_3-CeO_3 and Zn-TiO_2-CeO_3coating on mild steel. *The International Journal of Advanced Manufacturing Technology*, 85(5-8), 1419–1427. doi:10.1007/s00170-015-8063-5.

Refait, P., Grolleau, A. M., Jeannin, M., François, E., & Sabot, R. (2018). Corrosion of mild steel at the seawater/sediments interface: Mechanisms and kinetics. *Corrosion Science*, *130*, 76-84. doi: 10.1016/j.Corsci.2017.10.016.

Schmidt, D. P., Shaw, B. A., Sikora, E., Shaw, W. W., & Laliberte, L. H. (2006) Corrosion protection assessment of sacrificial coating systems as a function of exposure time in a marine environment. *Progress in Organic coatings*, 57(4), 352-364. doi: 10.1016/j.porgcoat.2006.09.021.

Sulpis, O., Agrawal, P., Wolthers, M., Munhoven, G., Walker, M., & Middelburg, J. J. (2022) Aragonite dissolution protects calcite at the seafloor. *Nature Communications*, 13(1), 1104. doi: 10.1038/s41467-022-28711-z.

Wang, J., Ji, C., Cui, S., & Jung, I. H. (2024) Thermodynamic study of the Ca-Cu-Zn ternary system with key experimental measurements. *Journal of Alloys and Compounds,* 970, 172509. doi: 10.1016/j.jallcom.2023.172509

Wang, K. (2025) Corrosion Behavior of Electrodeposited Zn–Co and Zn–Co–Mo Coatings on Mild Steel in NaCl Solution. *International Journal of Electrochemical Science*, 20(11), 101208. doi: 10.1016/j.ijoes.2025.101208.

Wei, Z., Chen, Z., Wang, Y., Yang, X., Li, D., Wu, Z., ... & Zhi, C. (2025) Catalytic electrolytes enable fast reaction kinetics and temperature adaptability for aqueous zinc-bromine flow batteries. *Nature Communications*, 16(1), 10097. doi: 10..1038/s41467-025-65047-w.

Wu, J., Zhang, D., Wang, P., Cheng, Y., Sun, S., Sun, Y., & Chen, S. (2016) The influence of Desulfovibrio sp. and Pseudoalteromonas sp. on the corrosion of Q235 carbon steel in natural seawater. *Corrosion Science*, 112, 552-562. doi: 10.1016/j.corsci.2016.04.047.

Xu, D., Li, Y., Song, F., & Gu, T. (2013) Laboratory investigation of microbiologically influenced corrosion of C1018 carbon steel by nitrate reducing bacterium Bacillus licheniformis. *Corrosion Science*, 77, 385-390. doi: 10.1016/j.corsci.2013.07.044.

Yang, Z., Shi, D., Wen, B., & Melnik, R. (2012) Structural, elastic, electronic properties and heats of formation of Ca–Zn intermetallics from first principles calculations. *Journal of alloys and compounds*, 524, 53-58. doi: 10.1016/j.jallcom.2012.02.075.